RESEARCH PAPER

# Structural and Luminescence Properties of $SnO_2$ Nanostructures Synthesized by a Porcine Gelatin-Assisted Route

**Arian Heidar Alaghband[1], Azam Moosavi[1,*], Saeid Baghshahi[2], Ali Khorsand Zak[3]**

* *a-moosavi@srbiau.ac.ir, az_moosavi@yahoo.com*

[1] Department of Materials Engineering, Science and Research Branch, Islamic Azad University, Tehran, Iran

[2] Engineering Department, Imam Khomeini International University, Qazvin, Iran

[3] Nanotechnology lab., Esfarayen University of Technology, Esfarayen, North Khorasan, Iran

**Received: June 2021** **Revised: July 2021** **Accepted: September 2021**

***DOI: 10.22068/ijmse.2287***

***Abstract:*** *Porous nanostructured $SnO_2$ with a sheet-like morphology was synthesized through a simple green substrate-free gelatin-assisted calcination process using Tin tetracholoride pentahydrate as the $SnO_2$ precursor and porcine gelatin as the template. Crystalline phase, morphology, microstructure, and optical characteristics of the as-prepared material were investigated using X-ray diffraction (XRD), Field emission scanning electron microscopy (FESEM), UV-visible absorption, and Photoluminescence spectroscopy (PL), respectively. XRD patterns of all the samples revealed the presence of a tetragonal crystalline structure with no other crystalline phase. Moreover, the synthesized hierarchical sheets assembled with nanoparticles displayed a large surface area and porous nanostructure. The calculated optical band gap energy varied from 2.62 to 2.87 eV depending on the calcination temperature. Finally, photoluminescence spectra indicated that the nanostructured $SnO_2$ exhibited an intensive UV-violet luminescence emission at 396 nm, with shoulders at 374, violet emission peaks at 405 and 414 nm, blue-green emission peak at 486 nm, green emission peak at 534 nm and orange emission peak at 628 nm.*

***Keywords:*** *$SnO_2$, Gel drying, Porcine gelatin, Sheet-like morphology, Optical properties, Photoluminescence.*

## 1. INTRODUCTION

Hierarchical self-assembly of micro/nanostructures with specific morphology have widespread potential applications in various fields of Materials Science [1, 2]. For example, nanostructured $SnO_2$ as one of the semiconductor materials is widely used in solar cells, transparent conductive electrodes, gas sensors, and lithium-anode materials [3-6]. $SnO_2$ has a wide band gap (3.62 eV) at room temperature. It also shows distinguished electrical, optical, and electrochemical properties, which have drawn significant attention on the applications. Many studies have been conducted to synthesize $SnO_2$ hierarchical structures in a controlled way. Among various approaches to synthesize inorganic materials, addition of surfactants as a structure-directing agent has attracted considerable attention [7-9]. Surfactants have been always used as additives modifying particle morphologies as well as sizes and crystal phases of nanostructured materials. The nucleation and growth of inorganic materials are controlled by the addition of surfactants, which regularly make the formation of hierarchical structure possible [8-11]. Gelatin is a natural protein with a triple-helix structure derived from collagen (the main structural protein being able to be dissolved in hot water and transformed to a random coil with series of repeating amino acids ($-NH_2$ and –COOH)). These functional groups may act as a complexing agent allowing Sn cations to disperse and form porous nanostructures [7, 12-13]. Commercial gelatin is also obtained from bovine and porcine (approximately 90% of gelatin comes from porcine) [12]. In addition, this biological material can make an effective additive for the fabrication of nanostructured inorganic materials in aqueous solutions. Recently, the crystal growth of metal oxides from an aqueous solution has captured much interest to fabricate various controlled nanostructures at near room temperature [8, 11, 14]. Among various methods for the preparation of nanostructured $SnO_2$ with different morphologies, such as nanospheres, nanosheets, nanorods, nanobelts, and nanowires [1, 15-16], a simple green gel-drying method by using gelatin as a soft template to modify the morphology and properties of $SnO_2$ is still interesting and challenging.

In the present study, we reported the synthesis of porous sheet-like $SnO_2$ nanostructures using porcine gelatin via a simple gel-drying method. A

$SnO_2$ hierarchical structure with a large surface and porous nanostructure is found to be built from nanoparticles. We also investigated the microstructural size, strain distribution, morphology, and optical properties of the prepared products.

## 2. EXPERIMENTAL PROCEDURE

To prepare hierarchical $SnO_2$ nanostructures, Tin tetracholoride pentahydrate ($SnCl_4.5H_2O$, 98% purity, Fluka) and porcine gelatin (type A, 90-100 Bloom, Sigma Aldrich, G6144) were used without further purification. All aqueous solutions were prepared with distilled water. To do so, firstly, 4 g porcine gelatin was dissolved in 60 mL of distilled water at about 40ºC. Secondly, 2 g $SnCl_4.5H_2O$ was dissolved into 20 mL distilled water under stirring; and added to the gelatin solution. Thirdly, the stirring aqueous solution was heated at 80ºC for 2 h until it transformed to a thick brown gel. The resulting gel was dried and calcined at different temperatures of 650, 700, and 750ºC for 2 h to obtain nanostructured $SnO_2$ [17]. Next, the obtained puffy gray powder was softly ground using agate mortar and pestle.

Then, X-ray diffraction (XRD, Siemens D500, Cu Kα radiation, λ= 1.5406 Å) analysis was performed to identify the crystalline phases. The crystallite size and lattice strain were also estimated from the resultant spectra using the Williamson-Hall method. Afterwards, the structural and morphological analyses of the powders were carried out with field-emission scanning electron microscopy (FESEM, MIRA3 TESCAN) by means of an energy dispersive X-ray spectrometer (EDS). UV-visible absorption spectra were recorded in the wavelength range of 200-800 nm using UV-VIS-NIR spectrophotometer (PerkinElmer, Model Lambda 25). Finally, the room temperature photoluminescence properties of the samples were measured by the Perkin Elmer Lambda 25 LS5 spectrometer using a xenon lamp laser as a source of stimulation with a wavelength of 320 nm.

## 3. RESULTS AND DISCUSSION

### 3.1. Structure and morphology

Figure 1 illustrates the X-ray diffraction patterns of the prepared samples calcined at 650, 700, and 750ºC. All the patterns confirmed that tetragonal rutile structure of $SnO_2$ (JCPDS card, No. 41-1445, space group: P42/mnm) formed without any other phases or detectable impurity.

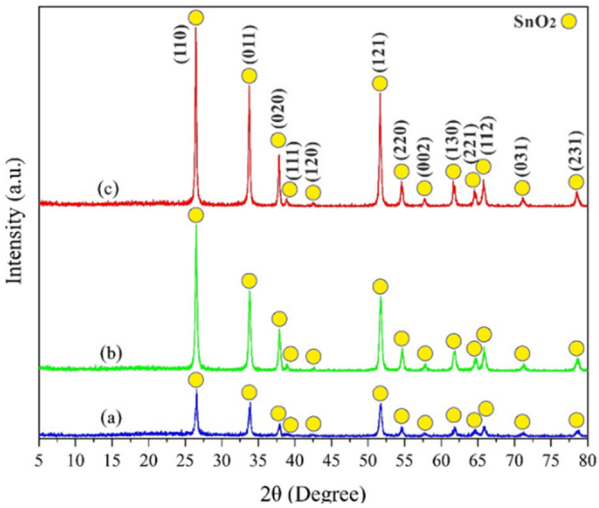


**Fig. 1.** XRD patterns of sheet-like $SnO_2$ calcined at (a) 650℃, (b) 700℃, and (c) 750℃.

The important point was that by increasing the temperature, the diffraction peaks became gradually sharper and the crystallinity of the $SnO_2$ hierarchical nanostructures were improved. (110) planes had the highest diffraction intensity and {110} are the most stable planes [18]. This indicated that gelatin could be an effective material for fabricating sheet-like $SnO_2$ via aqueous routes [17]. Moreover, to study the effect of porcine gelatin on microstructure parameters, the crystallite size and the micro-strain were estimated from the resultant patterns by Williamson-Hall method (Table 1). The effect of calcination temperature on the micro-strain estimated from the Williamson-Hall method showed that higher temperature decrease micro-strain contribution.

**Table 1.** The results of Williamson-Hall method.

| Calcination Temperature (ºC) | Mean crystallite size (nm) | Micro-strains |
|---|---|---|
| 650 | 26 | 0.0039 |
| 700 | 29 | 0.0024 |
| 750 | 38 | 0.0014 |

Figure 2 shows the morphologies of the as-synthesized product at different temperatures (650, 700, and 750ºC) and magnifications. The low magnification FESEM images provided a

general morphology with a 3D hierarchical nanostructure composed of abundant porous sheet-like morphologies with a large surface diameter (diameter of several micrometers). The shapes and sizes of the grains changed by increasing temperature so that less agglomeration happened at 650ºC and raising the temperature up to 700 and 750ºC resulted in more agglomeration and subsequently large grains and rough surfaces. Large porous surface provide a higher specific surface, containing a great quantity of active sites for improving adsorption. Moreover, Fig. 2(f) illustrates the high magnification FESEM image, which obviously demonstrates that assembled $SnO_2$ nanoparticles are distributed to form the large sheets. The morphology of micro-sheets also confirmed agglomeration of the grains. This grain agglomeration could account for nano-sized grains formation via the gel-drying synthesis method (Table 1). Further, results showed that the presence of porcine gelatin had a significant influence on $SnO_2$ morphology and proper amount of gelatin played an important role in obtaining hierarchical $SnO_2$ nanostructures without substrates [11, 14, 17]. This process verified that gelatin could serves as a structure-directing agent [8]. Therefore, the gelatin-based synthesis method known as a low-cost, green and facile process could be interesting to obtain texture and anisotropy of the $SnO_2$ crystal shape [17]. Gelatin is a natural organic material capable of being dissolved in hot water and acts as a soft template. Abundant -COOH and $–NH_2$ existing in gelatin coordinate with Sn ions [7]. Moreover, the interaction between molecular chains of gelatin offers an opportunity of self-assembly to obtain hierarchical structure [7, 17].

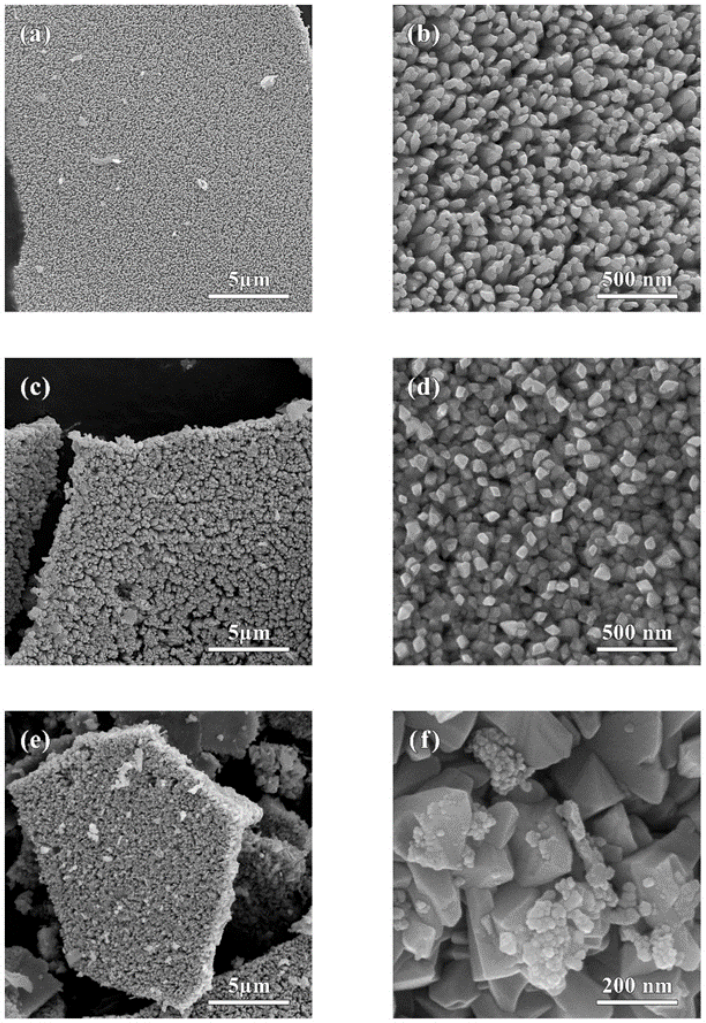


**Fig. 2.** SEM micrographs of sheet-like $SnO_2$ calcined at different temperatures and magnifications at (a, b) 650℃, (c, d) 700℃, and (e, f) 750℃.

Hierarchical $SnO_2$ nanostructures are obtained from self-oriented attachment of nano-grains to gelatin [10]. The formation of nanostructures occurs through nucleation and growth of $SnO_2$ particles. When the temperature increases, the grains grow faster. Additionally, higher temperature promotes gelatin oxidation and weight loss [19], to form porous 3D nanostructured $SnO_2$. On the other hand, the crystallized $SnO_2$ consists of large polycrystalline agglomerates composed of round-shaped nanoparticles. In the present study, we also found that decomposition of gelatin and formation of nanostructured $SnO_2$ start at about 650ºC (Fig. 1(a)) and heat treatment through higher temperatures (700 and 750ºC) increases the size of the nanoparticles (Table 1).

The possible formation process of hierarchical $SnO_2$ nanostructures is depicted schematically in Fig.3.

Furthermore, a typical EDS spectrum of the sheet-like $SnO_2$ calcined at 700 and 750ºC (Fig. 4) showed that in addition to Sn and O elements, N existed in the crystals. It is suspected that more temperature would be required for complete decomposition of gelatin. A cross-section FESEM image of $SnO_2$ sheets are shown in Fig. 5 to perceive the thickness at different temperatures. In this figure, we can notice that apart from the shape and size of grain, increasing the temperature had a direct effect on the thickness of the sheet-like $SnO_2$, nanostructured $SnO_2$ with average thickness about 390 nm changed to 608 nm.

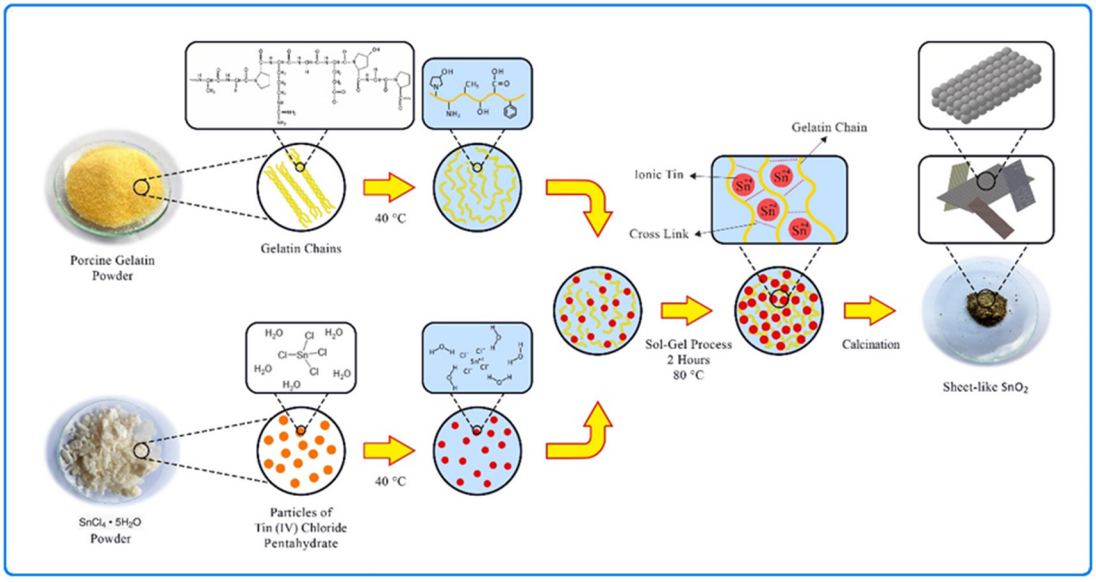


**Fig. 3.** Schematic formation process of hierarchical $SnO_2$ nanostructures.

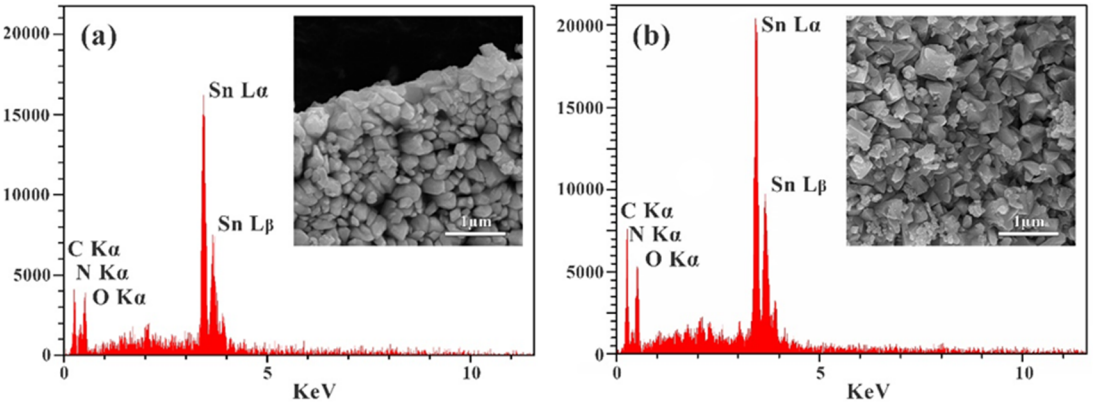


**Fig. 4.** Energy dispersive spectra (EDS) analysis of samples at (a) 700℃, and (b) 750℃.

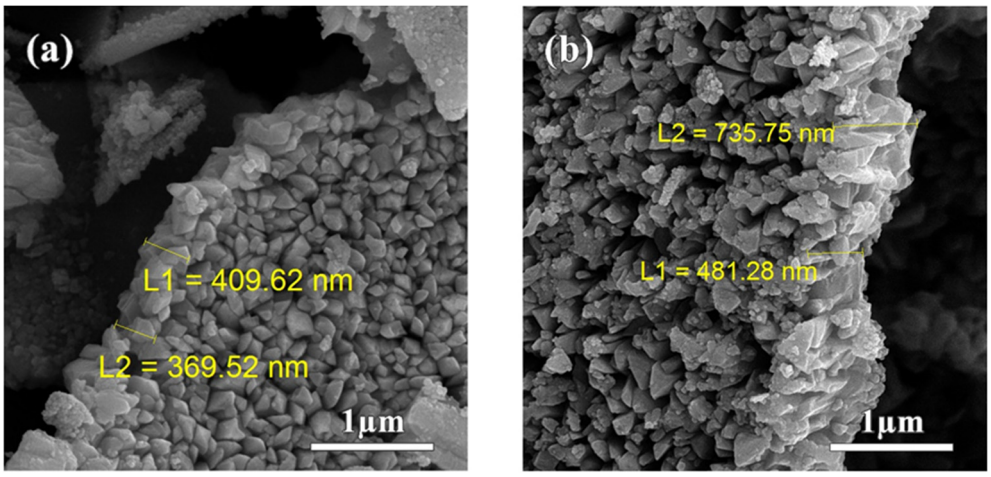


**Fig. 5.** Cross-section of the nanostructured $SnO_2$ at (a) 700℃, and (b) 750℃.

### 3.2. Optical properties

#### *3.2.1. UV–visible spectroscopy*

The UV-vis spectra of the sheet-like $SnO_2$ samples were further obtained in the wavelength range of 200 to 800 nm. As can be seen in Fig. 6, a strong absorption has taken place in the ultraviolet region at 273 nm and there is a good transparency in the visible region. Meanwhile, the optical band gap of the sheet-like $SnO_2$ nanostructures were determined using Tauc's plot, by the extrapolation of linear part of curve $(\alpha h\nu)^2$ versus photon energy ($h\nu$) to zero absorption, $\alpha$ is the absorption coefficient. The optical band gaps were found to be lower than the reported value of 3.62 eV for bulk $SnO_2$ particles (Table 2).

According to the quantum confinement effect, band gaps depend on the crystallite size so that they increase with decreasing crystallite size. Moreover, as shown in Table 1, the calculated size of the nanoparticles forming the sheet-like $SnO_2$ is about 29 nm at 700ºC.

According to the previous studies, the red shift from bulk band gap may be due to the large morphology of the sheets, residual strain, and the defects [20-22]. Also, large amount of oxygen vacancies with different charge states ($V_O^0$, $V_O^+$ and $V_O^{++}$) could be formed within the crystal.

These oxygen vacancies could in turn give rise to donor and acceptor levels within the band gap [23-28]. For instance, $V_O^0$ acts as a shallow donor, which lies at 0.39 eV below the conduction band, while $V_O^+$ and $V_O^{++}$ act as acceptor levels located at 0.84 and 0.18 eV above the valence band, respectively [28]. These levels further act as radiative centers in PL analysis [24].

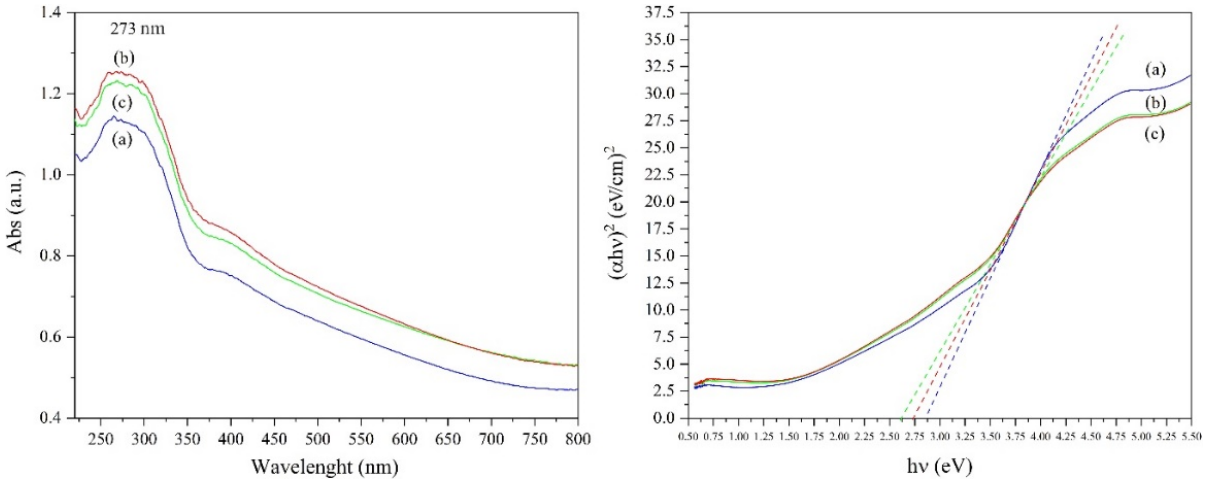


**Fig. 6.** Left: absorption spectra; right: Tauc plots of nanostructured $SnO_2$ at (a) 650℃, (b) 700℃, and (c) 750℃.

**Table 2.** The calculated band gap energy ($E_g$) from absorption edge.

| Calcination Temperature (ºC) | The optical band gap (eV) |
|---|---|
| 650 | 2.87 |
| 700 | 2.74 |
| 750 | 2.62 |

### *3.2.2. Photoluminescence*

In the current work, we measured the photoluminescence (PL) spectra of the nanostructured $SnO_2$ samples to evaluate both optical properties and crystal defects with an excitation wavelength of 320 nm (3.87 eV). As can be perceived in Fig. 7, the characteristic peak intensity of the product at 700ºC is higher than that of other temperatures. We can also notice that the sheet-like $SnO_2$ obtained at 700ºC exhibits UV emission peak at 374 nm (3.32 eV) and UV-violet emission peak at 396 nm (3.13 eV). In Fig.7, the PL spectrum also shows two strong visible-light emission peaks centered at 405 nm (violet emission, 3.06 eV) and 414 nm (purple emission, 2.99 eV). Since the energy corresponding to all these emissions was found to be higher than that of the optical band gap (2.74 eV), it can be assigned to the direct recombination of an electron in Sn 4p band and a hole in the O 2p valance band [24-28], meaning that the prepared sheet-like $SnO_2$ nanostructures were suitable UV light emitters potential to be used for optical applications, such as photo-detectors and light-emitting diodes [27].

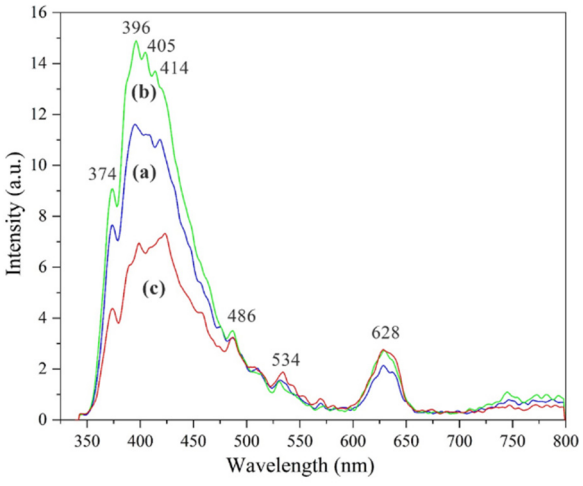


**Fig. 7.** Room temperature PL spectra of nanostructured $SnO_2$ at (a) 650℃, (b) 700℃, and (c) 750℃.

The energy of other weak peaks at 486 nm (blue-green emission, 2.55 eV), 534 nm (green emission, 2.32 eV), and 628 nm (orange emission, 1.97 eV) are particularly smaller than the band gap energy, therefore they can be attributed to defect levels in $SnO_2$ band gap [24-28]. As mentioned before, transition in defect states, above all the oxygen vacancies with different charge states $V_O^0$, $V_O^+$ and $V_O^{++}$ as radiative centers, causing visible light emissions. Moreover, the electron transition from conduction band to $V_O^+$ and $V_O^{++}$ levels nearly corresponded to the orange and blue-green emissions, respectively. Besides, the electron transition from $V_O^0$, as a shallow donor level, to the valence band matched to green emission.

## 4. CONCLUSIONS

In summary, a simple gel-drying method was developed for the synthesis of the $SnO_2$ with porous sheet-like morphology by heating up to 650, 700, and 750ºC. Gelatin played an essential role in obtaining large-area $SnO_2$ sheets. The obtained samples were polycrystalline with tetragonal crystal structure. The reduction of optical band gap energy of sheet-like $SnO_2$ in comparison to the bulk value could be due to the crystallite size of the films, residual strain and oxygen vacancies. Also, the PL property of sheet-like $SnO_2$ was analyzed based on the PL spectrum, which were composed of an intensive UV-violet peak at 396 nm, and other peaks at 374, 405, 414 nm, which can be all assigned to the direct recombination of an electron in Sn 4p band and a hole in the O 2p valance band. Three peaks at 486, 534, and 628 nm may be attributed to defect levels in $SnO_2$ band gap.

## REFERENCES:

[1] Liu, J., Tang, X. C., Xiao, Y. H., Jia, H., Gong, M. L. and Huang, F. Q., “Porous sheet-like and sphere-like nano-architectures of $SnO_2$ nanoparticles via a solvent-thermal approach and their gas-sensing performances.” Mater. Sci. Eng. B., 2013, 178, 1165–1168.

[2] Wan, W., Li,Y., Ren, X., Zhao,Y., Gao, F. and Zhao, H., “2D $SnO_2$ Nanosheets: Synthesis, Characterization, Structures,

and Excellent Sensing Performance to Ethylene Glycol." Nanomaterials, 2018, 8, 8020112.

[3] Chappel, S. and Zaban, A., "Nanoporous $SnO_2$ electrodes for dye-sensitized solar cells: improved cell performance by the synthesis of 18nm $SnO_2$ colloids." Sol. Energy Mater. Sol. Cells., 2002, 71, 141–152.

[4] Lee, J., Kim, N. H. and Park, Y., "Characteristics of $SnO_2$: Sb Films as Transparent Conductive Electrodes of Flexible Inverted Organic Solar Cells", J. Nanosci. Nanotechnol., 2016, 16, 4973–4977.

[5] Kuang, X., Liu, T., Shi, D., Wang, W., Yang, M., Hussain, S., Peng, X. and Pan, F., "Hydrothermal synthesis of hierarchical $SnO_2$ nanostructures made of superfine nanorods for smart gas sensor." Appl. Surf. Sci., 2016, 364, 371–377.

[6] Hwang, S. M., Lim,Y. G., Kim, J. G., Heo, Y. U., Lim, J. H., Yamauchi,Y., Park, M. S., Kim,Y. J., Dou, S. X. and Kim, J. H., "A case study on fibrous porous $SnO_2$ anode for robust, high-capacity lithium-ion batteries." Nano Energy., 2014, 10, 53–62.

[7] Du, H., Huang, K., Dong,W. and Geng, B., "A general gelatin-assisted strategy to hierarchical porous transition metal oxides with excellent lithium-ion storage." Electrochim. Acta., 2018, 279, 66–73.

[8] Fang, K. M., Wang, Z. Z., Zhang, M., Wang, A. J., Meng, Z. Y. and Feng, J. J., "Gelatin-assisted hydrothermal synthesis of single crystalline zinc oxide nanostars and their photocatalytic properties." J. Colloid Interface Sci. 2013, 402, 68–74.

[9] Stroyuk,O. L., Rayevska,O. Y., Shvalagin,V. V., Kuchmiy, S. Y., Bavykin, D. V., Streltsov, E. A. and Poznyak, S. K., "Gelatin-templated mesoporous titania for photocatalytic air treatment and application in metal chalcogenide nanoparticle-sensitized solar cells." Photochem. Photobiol. Sci., 2013, 12, 621–625.

[10] Tseng,Y. H., Lin, H. Y., Liu M. H., Chen,Y. F. and Mou, C. Y., "Biomimetic Synthesis of Nacrelike Faceted Mesocrystals of ZnO−Gelatin Composite." J. Phys. Chem. C., 2009, 113, 18053–18061.

[11] Bauermann, L. P., Campo, A., Bill, J. and Aldinger, F., "Heterogeneous Nucleation of ZnO Using Gelatin as the Organic Matrix." Chem. Mater., 2006, 18, 2016–2020.

[12] Nemati, M., Oveisi, M. R., Abdollahi, H. and Sabzevari, O., "Differentiation of bovine and porcine gelatins using principal component analysis." J. Pharm. Biomed. Anal., 2004, 34, 485–492.

[13] Zhang, G., Liu, T., Wang, Q., Chen, L., Lei, J., Luo, J., Ma, G. and Su, Z., "Mass spectrometric detection of marker peptides in tryptic digests of gelatin: A new method to differentiate between bovine and porcine gelatin." Food Hydrocoll., 2009, 23, 2001–2007.

[14] Uchiyama, H., Nakanishi, S. and Kozuka, H., "Hydrothermal synthesis of nanostructured SnO particles through crystal growth in the presence of gelatin." J. Solid State Chem., 2014, 217, 87–91.

[15] Luo, S., Fan, J., Liu, W., Zhang, M., Song, Z., Lin, C., Wu, X. and Chu, P. K., "Synthesis and low-temperature photoluminescence properties of $SnO_2$ nanowires and nanobelts." Nanotechnology., 2006, 17, 1695–1699.

[16] Duan, J., Liu, X., Han, Q. and Wang, X., "Controlled morphologies and optical properties of ZnO films and their photocatalytic activities." J. Alloys Compd., 2011, 509, 9255–9263.

[17] Bagherian, S. and Zak, A. K., "X-ray

peak broadening and optical properties analysis of $SnO_2$ nanosheets prepared by sol-gel method." Mater. Sci. Semicond. Process., 2016, 56, 52–58.

[18] Li, T., Zeng, W., Long, H. and Wang, Z., "Nanosheet-assembled hierarchical $SnO_2$ nanostructures for efficient gas-sensing applications." Sensors Actuators B Chem., 2016, 231, 120–128.

[19] Kasuya, A., Paulista, A., Alencar, A. and Braga,T., "Gelatin Template Synthesis of Aluminum Oxide and/or Silicon Oxide Containing Micro/Mesopores Using the Proteic Sol-Gel Method." J. Nanomater., 2017, 2017, 1–11.

[20] Mariammal, R. N., Ramachandran, K., Renganathan, B. and Sastikumar, D., "On the enhancement of ethanol sensing by CuO modified $SnO_2$ nanoparticles using fiber-optic sensor." Sensors Actuators B Chem., 2012, 169, 199–207.

[21] Kamble, V. B. and Umarji, A. M., "Defect induced optical bandgap narrowing in undoped $SnO_2$ nanocrystals." AIP Adv., 2013, 3, 82120.

[22] Arya, S., Riyas, M., Sharma,A., Singh, B., Prerna, Bandhoria, P., Khan, S. and Bharti,V., "Electrochemical detection of ammonia solution using tin oxide nanoparticles synthesized via sol–gel route." Appl. Phys. A., 2018, 124, 538.

[23] Kang, S. Z., Wu, T., Li, X. and Mu, J., "A facile gelatin-assisted preparation and photocatalytic activity of zinc oxide nanosheets." Colloids Surfaces A Physicochem. Eng. Asp., 2010, 369, 268–271.

[24] Gu, F., Wang, S. F., Lü, M. K., Zhou, G. J., Xu, D. and Yuan, D. R., "Photoluminescence Properties of SnO2 Nanoparticles Synthesized by Sol−Gel Method." J. Phys. Chem. B., 2004, 108, 8119–8123.

[25] Xu, M., Ruan, X., Yan, J., Zhang, Z., Yun, J., Zhao, W., Li, T. and Shi,Y., "Synthesis, growth mechanism, and photoluminescence property of hierarchical $SnO_2$ nanoflower-rod arrays: an experimental and first principles study." J. Mater. Sci., 2016, 51, 9613–9624.

[26] Wang, X., Wang, X., Di, Q., Zhao, H., Liang, B. and Yang, J., "Mutual Effects of Fluorine Dopant and Oxygen Vacancies on Structural and Luminescence Characteristics of F Doped $SnO_2$ Nanoparticles." Materials (Basel)., 2017, 10, 1398.

[27] Teldja, B., Noureddine, B., Azzeddine, B. and Meriem,T., "Effect of indium doping on the UV photoluminescence emission, structural, electrical and optical properties of spin-coating deposited $SnO_2$ thin films." Optik (Stuttg)., 2020, 209, 164586.

[28] Mrabet, C. Boukhachem, A., Amlouk, M. and Manoubi, T., "Improvement of the optoelectronic properties of tin oxide transparent conductive thin films through lanthanum doping." J. Alloys Compd., 2016, 666, 392–405.